The Astrophysical Journal, 864:21 (12pp), 2018 September 1 https://doi.org/10.3847/1538-4357/aad2d9

Quite-Sun and Coronal Hole in Mg II k Line as Observed by *IRIS*

Pradeep Kayshap[1], Durgesh Tripathi[2], Sami K. Solanki[3,4], and Hardi Peter[3]
[1] Group of Astrophysics, University of Maria Curie-Skłodowska, ul. Radziszewskiego 10, 20-031 Lublin, Poland
[2] Inter-University Centre for Astrophysics, Post Bag—4, Ganeshkhind, Pune-411007, India; durgesh@iucaa.in
[3] Max-Planck Institute for Solar System Research, Justus-von-Liebig-Weg 3, D-37077, Göttingen, Germany
[4] School of Space Research, Kyung Hee University, Yongin, Gyeonggi-Do, 446-701, Republic of Korea
Received 2018 March 21; revised 2018 June 18; accepted 2018 July 9; published 2018 August 27

Abstract

Coronal hole (CH) regions are dark in comparison to the quiet Sun (QS) at coronal temperatures. However, at chromospheric and transition region temperatures, the QS and CHs are hardly distinguishable. In this study, we have used the Mg II 2796.35 Å spectral line recorded by the *Interface Region Imaging Spectrometer* (*IRIS*) to understand the similarities and differences in the QS and CH at chromospheric levels. Our analysis reveals that the emission from Mg II k3 and k2v that originates in the chromosphere is significantly lower in CH than in QS for the regions with similar magnetic field strength. The wing emissions of Mg II k that originates from the photospheric layer, however, do not show any difference between QS and CH. The difference in Mg II k3 intensities between QS and CH increases with increasing magnetic field strength. We further studied the effects of spectral resolution on these differences and found that the difference in the intensities decreases with decreasing spectral resolution. For a resolution of 11 Å, the difference completely disappears. These findings are not only important for mass and energy supply from the chromosphere to the corona but also provides essential ingredients for the modeling of the solar spectral irradiance for the understanding of the Sun–climate relationships.

Key words: Sun: atmosphere – Sun: chromosphere – Sun: photosphere – Sun: UV radiation

1. Introduction

Dark regions on the Sun at coronal temperatures are termed coronal holes (CHs), which can be observed both at low heliographic latitudes (primarily around solar activity maximum) and at the solar polar caps (primarily around solar activity minimum). At these temperatures, the emission from CHs is significantly lower than from other regions such as quiet Sun (QS) and active regions (see, e.g., Waldmeier 1975), making them distinguishable from other areas. The difference between the two types of structures is thought to be a product of the different magnetic topology, with field lines being mainly closed, loop-like structures in the QS, while they possess an open funnel-like configuration in CHs. However, the QS and CHs are not clearly distinguishable in intensity images taken at chromospheric temperatures except for in He I and He II lines, whose formation is very sensitive to EUV radiation from the corona, as well as to energetic electrons coming down from the corona, e.g., in the form of heat conduction (see, e.g., Avrett et al. 1994; Andretta & Jones 1997; Centeno et al. 2008; Leenaarts et al. 2016). Therefore, the differences between CHs and the QS seen in He I and He II lines are likely linked to the differences in the overlying transition region (TR) and corona. Based on the Solar Ultraviolet Measurements of Emitted Radiation (SUMER, Wilhelm et al. 1995) observations on board the *Solar and Heliospheric Observatory* (*SoHO*), Wilhelm et al. (2000) reported that the radiance of the He I 584 Å line is about 30% lower in CHs than in the QS. The differences have also been noted in other parameters such as Doppler shift and line widths (see, e.g., Dupree et al. 1996; Peter 1999b; Stucki et al. 2000, 2002).

The H and K lines of Ca II that represent the chromospheric emission are found to have the central intensities slightly enhanced in CH over QS (see, e.g., Teplitskaya et al. 2006, 2007). In another study, using multiple spectral lines from SUMER, Stucki et al. (2000) suggested that for cooler chromospheric lines like Ni II, the spread of intensities in CHs is larger than in the QS. However, this difference disappeared in TR lines, e.g., O IV. This behavior was reversed in coronal lines. Using the observations from the Coronal Diagnostics Spectrometer (Harrison et al. 1995) on board *SoHO*, it was found that the CHs and QS can be clearly distinguished only at temperatures higher than 7×10^5 K, ignoring the He lines (Stucki et al. 2002). The weakness of such studies, particularly at chromospheric and TR temperatures is that they do not consider the strong dependence of radiance on magnetic flux. Thus, a difference in magnetic flux (or a distribution of the flux) in the CH relative to the QS could explain any differences found in the lower atmosphere. If, after taking any difference in magnetic flux into account there still is a difference between the intensity of chromospheric lines in CHs and the QS, it would suggest that the magnetic field plays an important role in heating the quiet chromosphere.

The fact that CHs are clearly visible in coronal, but not in chromospheric, radiation was explained by Wiegelmann & Solanki (2004) by the different density of long and high coronal loops, but the similar number of short, low cool loops in the QS and CHs. A clear difference in chromospheric thermal structure between the QS and CHs, other than in He lines, could indicate that the number density of short, cool loops is indeed different in CHs and the QS, or that the heating of such loops is less efficient in CHs.

The *Interface Region Imaging Spectrometer* (*IRIS*; De Pontieu et al. 2014) provides high spectral, spatial, and temporal resolution spectra in various spectral lines including the Mg II h and k lines. Therefore, such data provide an excellent opportunity to compare, for the first time, the properties of these lines and their behavior in QS and CH regions. In particular, it is unknown if the Mg II h and k lines have a different intensity in CHs than in the QS. If they do, it

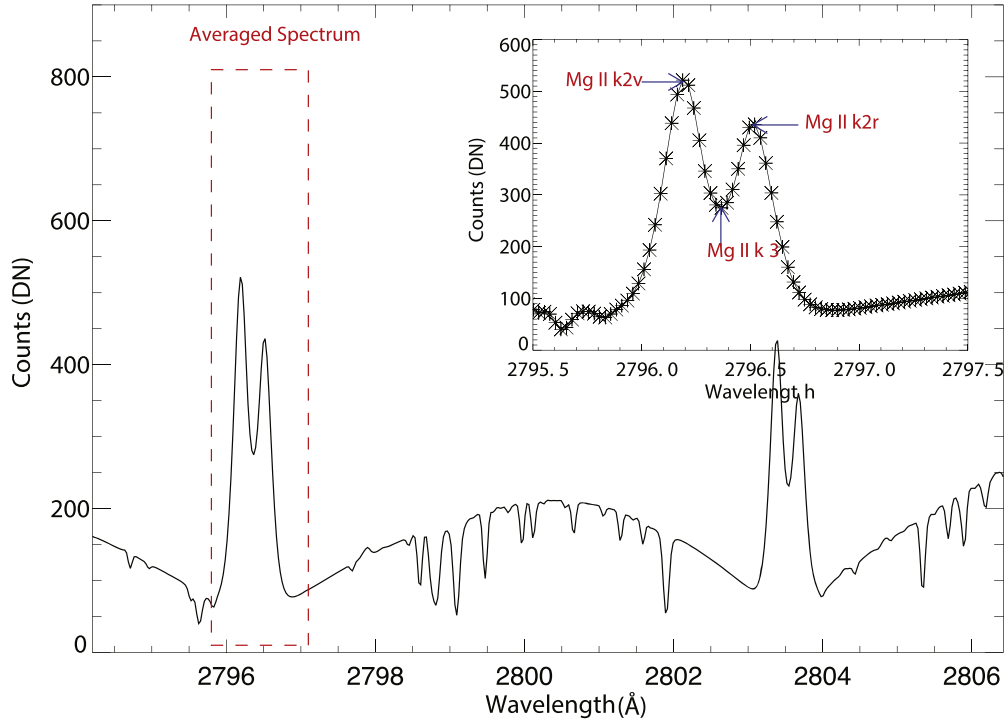

Figure 1. Averaged, over entire raster, spectrum obtained in the Mg II window of *IRIS* observation taken on 2015 November 14. The k-line is boxed in red and is also shown in the inset. The blue arrows in the inset locate the k2v and k2r peaks and the central absorption at k3.

Table 1
Summary of All Three Sets of Observations of the Quiet Sun (QS) and Coronal Holes (CH)

	Date (Time)		Field of View		τ [s]		μ		$B_{\rm LOS}/\mu$ [G]	
Data	QS	CH	QS	CH	QS	CH	QS	CH	QS	CH
Set 1	10.11.15(13:30:04)		129″ × 170″		15		0.81	0.88	10.06	10.64
Set 2	04.01.16 (04:54:38)	05.01.16 (14:50:33)	126″ × 130″	129″ × 173″	15	15	0.90	0.90	10.18	10.41
Set 3	18.12.14 (05:47:42)	29.11.14 (23:02:45)	34″ × 181.″0	126″ × 129.″0	30	30	0.88	0.81	19.44	16.98

Note. τ is the exposure time, μ is the cosine of the heliocentric angle, and $B_{\rm LOS}$ is the average LOS magnetic field.

would shed some light on either their formation mechanism, or on the difference in properties of the the middle-upper chromosphere in CHs and the QS. At present this layer is expected to be roughly similar in both types of magnetic topology. If a difference is found, then it would suggest that the chromosphere is at least partly magnetically heated and that the number density of small loops is different in the two regions.

The rest of the paper is structured as follows. The details of the observation and data analysis are presented in Section 2. In Section 3, we describe the observational findings of the present work. A discussion and conclusions are outlined in Section 4.

2. Observation and Data Analysis

In the present study, we have used observations recorded with *IRIS*, and the Atmospheric Imaging Assembly (AIA; Lemen et al. 2012) and the Helioseismic and Magnetic Imager (HMI; Scherrer et al. 2012) on board the *Solar Dynamics Observatory* (*SDO*). Since the primary aim of our study is to compare the radiance of the Mg II k line in QS and CH for magnetic elements with similar strength, it is important to consider the sets of observations where QS and CH are observed either in a single *IRIS* raster, or at least are observed at the same μ value (where μ is defined as $\mu = \cos\theta$, with θ being the heliographic longitude) sufficiently close in time, so that there is no degradation of the instrument response between the two observations. This is necessitated to avoid any bias introduced by the strong center to limb variation in the radiance in Mg II lines (see, e.g., Gouttebroze & Lemaire 1974; Avrett et al. 2013; Schmit et al. 2015). We have chosen sets of observations that fulfill these requirements for the study here. See Table 1 for the details of observations. One of the observations recorded on 2015 November 10, contained a portion of the QS as well as of a CH in a single raster. In the second and third sets of observations, the QS and CH were observed on two different dates, although at almost the same μ value. Here we concentrate on the detailed analysis of the first and second set of observations. Since the analysis, as well as the results of the third set are very similar to the first two cases, we have relegated the results obtained using set 3 to an Appendix.

The Mg II k spectral line (2796.35 Å) is an optically thick line, whose core is comprised of two peaks and a central

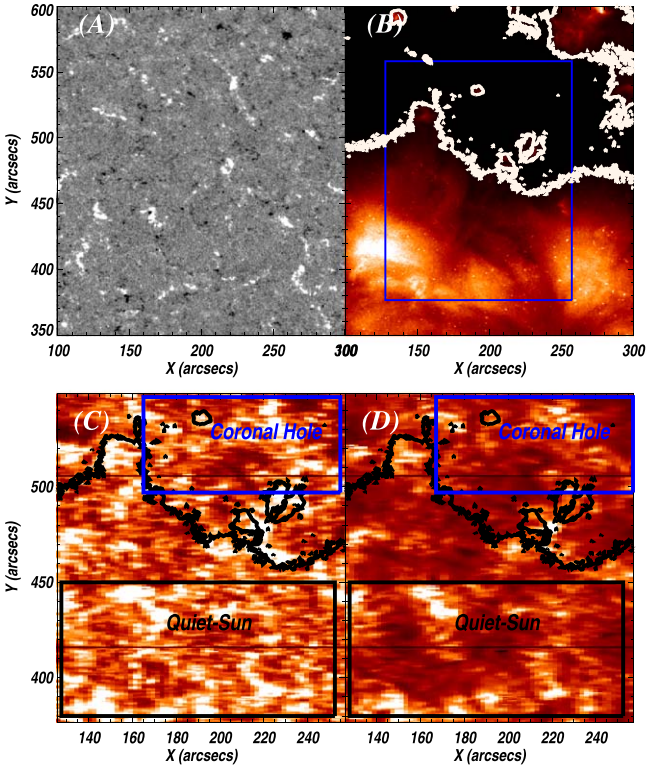

Figure 2. Region of interest for data set 1. HMI magnetogram (panel (A)) and AIA 193 Å image (panel (B)) showing a portion of the solar disk containing both the QS and CHs on 2015 November 10. The blue box overplotted on panel (B) represents the FOV of the *IRIS* raster. The *IRIS* intensity images obtained in Mg II k2v and Mg II k3 are shown in panels (C) and (D). The overplotted contours (at a level of 80 DN/s in the AIA 193 Å channel) in panels (B), (C), and (D) demarcate the boundary of the coronal hole and quiet Sun. The lower black and upper blue boxes in panels (C) and (D) represent the QS and CH regions, respectively, which are used for further analysis.

reversal except at a few locations, e.g., in sunspot umbrae. Figure 1 displays the spectrum in the Mg II window averaged over the entire raster recorded on 2015 November 14. The red box locates the k-line of Mg II that is also shown as an inset in Figure 1. The two peaks, i.e., k2v (the short wavelength peak) and k2r (the long wavelength peak), and the k3 (dip in the line intensity) are labeled (see Leenaarts et al. 2013, for more on nomenclature of the Mg II k lines).

The intensities in the k2 and k3 features of Mg II line are highly sensitive to magnetic field (Leenaarts et al. 2013). Therefore, we performed a pixel-to-pixel correlation between the intensity maps of k2 and k3 and the projected LOS magnetic field and performed a comparison among intensities obtained for k2v and k3 locations of the Mg II line in QS and CH for regions with similar magnetic field density. To find the Mg II k2 and k3 intensities, we have used the procedure "iris_get_mg_features.pro," which is described in Pereira et al. (2013) and Leenaarts et al. (2013).

To achieve the aims of this paper, we need to compare the radiance of the Mg II k line in QS and CH. To remove any bias due to different amounts of magnetic flux in the CH and QS regions studied, we compare the dependence of Mg II k intensity on pixel-averaged magnetic field strength. The latter value is taken from HMI magnetograms, which are recorded when the *IRIS* raster reaches its midpoint. This time will be referred to as the center time. The HMI data was rebinned as per *IRIS* resolution to overcome different pixel sizes and spatial resolutions of *IRIS* and HMI. For such an analysis it is mandatory to have near perfect coalignment between the magnetograms taken using HMI and the spectral images in Mg II line core obtained by *IRIS*. We have used cross-correlation to align *IRIS* and HMI images.

3. Observational Results

3.1. Data Set 1: Covering QS and CH in the Same Raster Map

On 2015 November 10, *IRIS* rastered a region that covered a portion of QS as well as a CH using a 64 step coarse raster (i.e., 2″ raster steps). Figure 2 displays the HMI magnetogram (panel (A)) recorded at the center time of the *IRIS* raster and a portion of the Sun's disk imaged by AIA in its 193 Å channel (panel (B)) on the same day. It is well established that CHs and the QS are easily distinguished in coronal emission. Therefore, we have used AIA 193 Å images to define the boundary between the QS and CHs. By manual inspection, we have found that a threshold of 80 DN/pix demarcates the boundary between QS and CH reasonably well, as outlined by white contours on the AIA 193 Å image (cf. panel (B); Figure 2). The blue box in panel (B) represents the region that was rastered by *IRIS*. It is clearly seen that the *IRIS* raster covered both the QS and CHs. Panels (C) and (D) are the maps representing the intensity at the (local) maximum and minimum of the spectral radiance of the Mg II line profile at the k2v peak and the k3 dip, respectively. Clearly, both in k2v and k3, the structures in the QS are very similar to those in the CH region, unlike in the 193 Å image. The same applies to the magnetic field obtained from HMI observations (panel (A)) that shows similar structure in CHs and the QS. For further quantitative analysis and comparison, we have selected the upper blue and the lower black boxes (shown in panels (C) and (D)) representing CHs and the QS, respectively. Figure 3 shows the distribution of magnetic field in the QS (black) and CHs (blue).

To compare the strength of the Mg II k line in QS and CH for regions with very similar spatially averaged magnetic field strength, we grouped regions within a constant bin of 0.05 based on their pixel-averaged $\langle B_{\rm LOS}\rangle/\mu$ on logarithmic scale as obtained from the HMI magnetogram. A logarithmic scale was used to have a sufficient number of pixels with high magnetic field. The number of Mg II profiles in each magnetic field bin are given in Table 2. The complete QS and CH fields of view (FOVs) marked by black and blue boxes in panels (C) and (D) of Figure 2, were divided into various bins covering pixel-averaged LOS magnetic field, $\langle B_{\rm LOS}\rangle/\mu$, from ∼2.0 Gauss up to ∼60.0 Gauss. We have excluded locations with higher magnetic field strength (i.e., more than 60 Gauss) as those are rare and introduce excessive scatter into the relationship at the high field end. The spectra at all the locations in a given magnetic field bin are then averaged. Figure 4 displays four averaged Mg II k line profiles for QS (blue) and CH (black) obtained in four bins of different $\langle B_{\rm LOS}\rangle/\mu$ as labeled in each panel. The plots clearly demonstrate that the Mg II line is stronger in QS than in the CH, when compared at the same magnetic field strength. Moreover, the difference in the k2 peaks and the k3 dip increases with increasing magnetic field.

We first investigate the relation of the coronal intensity to the magnetic field, which should show a clear difference between CHs and the QS. The upper panel in Figure 5 displays the scatter plot of the intensities in the QS (black) and CHs (black) based on the AIA 193 Å observations as a

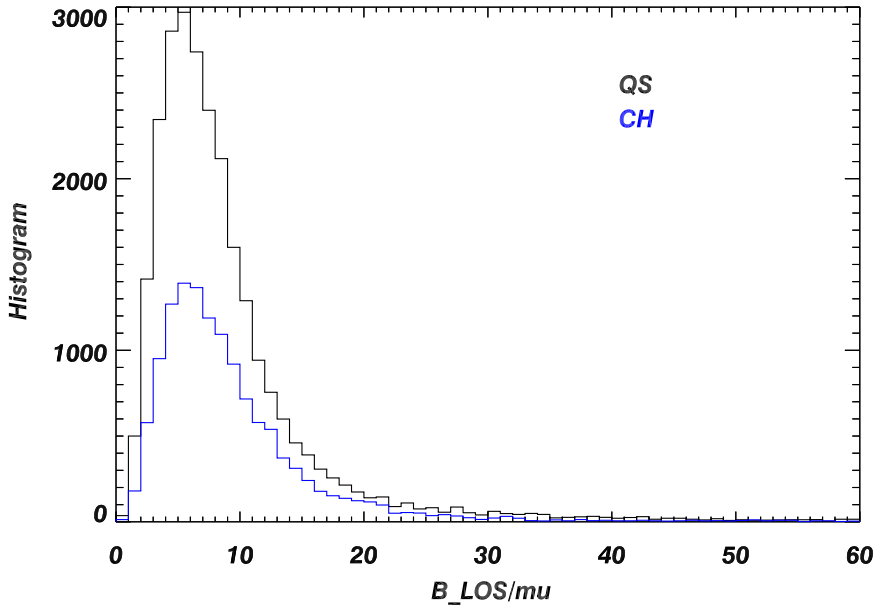

Figure 3. Distribution of the magnetic field in the QS and CHs as identified in Figure 2.

Table 2
Number of Mg II Profiles in Each Magnetic Field Bin

	Mg II k (No. of Profiles)	
B_LOS Bins	QS	CH
3.98–4.46	1658	772
4.46–5.01	1857	971
5.01–5.62	2030	1013
5.62–6.30	2072	1032
6.30–7.07	2059	1094
7.07–7.94	2064	1009
7.94–8.91	1740	894
8.91–10.00	1485	762
10.00–11.22	1125	680
11.22–12.58	923	484
12.58–14.12	716	369
14.12–15.84	567	301
15.84–17.78	411	254
17.78–19.95	310	156
19.95–22.38	262	111
22.38–25.12	208	76
25.12–28.18	178	61
28.18–31.62	157	39
31.62–35.48	111	36
35.48–39.81	113	33
39.81–44.66	80	47
44.66–50.12	71	33
50.12–56.32	60	30
56.32–63.09	53	33

function of $\langle B_{\rm LOS}\rangle/\mu$. The bottom panel shows the behavior of coronal intensities in the QS (black) and CHs (blue) as observed in 193 Å after averaging the intensities in each bin of $\langle B_{\rm LOS}\rangle/\mu$. As stated above we have selected a constant step of 0.08 $\langle B_{\rm LOS}\rangle/\mu$ for each bin. These plots demonstrate the difference in the QS and CHs that is clearly discernible (see panel (B) in Figure 2). The coronal QS intensities are a factor of more than four higher than those in the CH. The difference in the intensities first decreases and later increases with increasing $\langle B_{\rm LOS}\rangle/\mu$, although this may be by chance (poor statistics), as we shall see by comparing with the other data sets analyzed here.

The difference between CHs and the QS in Mg II is best illustrated by relating the intensity of the Mg II features to the magnetic field strength. Figures 6 and 7 display scatter plots of intensities (top panel), and average intensities in different magnetic field bins (bottom panel) as a function of $\langle B_{\rm LOS}\rangle/\mu$ of the QS (black) and CH (blue) regions shown in Figure 2 for the k3 reversal and the k2v peak, respectively. The histograms of intensities are plotted in the middle panels. The scatter plots show that although most of the points overlap for similar magnetic field strength, there are regions in QS that are brighter than all regions in the studied CH. The histograms of QS and CH intensities in Figures 6 and 7 confirm that there is a large overlap (although it is smaller than the histograms suggest, as the dependence on $\langle B_{\rm LOS}\rangle/\mu$ enhances it). The average QS intensities in the same magnetic field bins are larger than in CHs, and this difference increases with increasing magnetic field for both k3 as well as k2v. At even higher magnetic fields, a decrease in the difference is seen. We attribute this to poor statistics, as there are very few locations with magnetic field higher than 50 Gauss. However, we cannot rule out that the stronger network elements display similar brightness in CHs and the QS, while it is only the weaker elements that are different. We emphasize here that these differences are not visible when considering the images directly by eye.

3.2. Data Set 2: QS and CH Observed in Separate Rasters

The second data set is comprised of two coarse rasters, one of the QS taken on 2016 January 4, the other of a CH taken on 2016 January 5. The time difference between QS and CH observations is just ∼36 hr, which is small enough to leave our results unaffected by instrument degradation. Figure 8 displays a portion of the Sun imaged by AIA 193 Å on January 4, showing the observed QS region (panel (A)) and on January 5 showing CH (panel (B)). Overplotted green boxes on both the images mark the areas covered by *IRIS*. The QS and CH regions mapped by *IRIS* were located at very similar

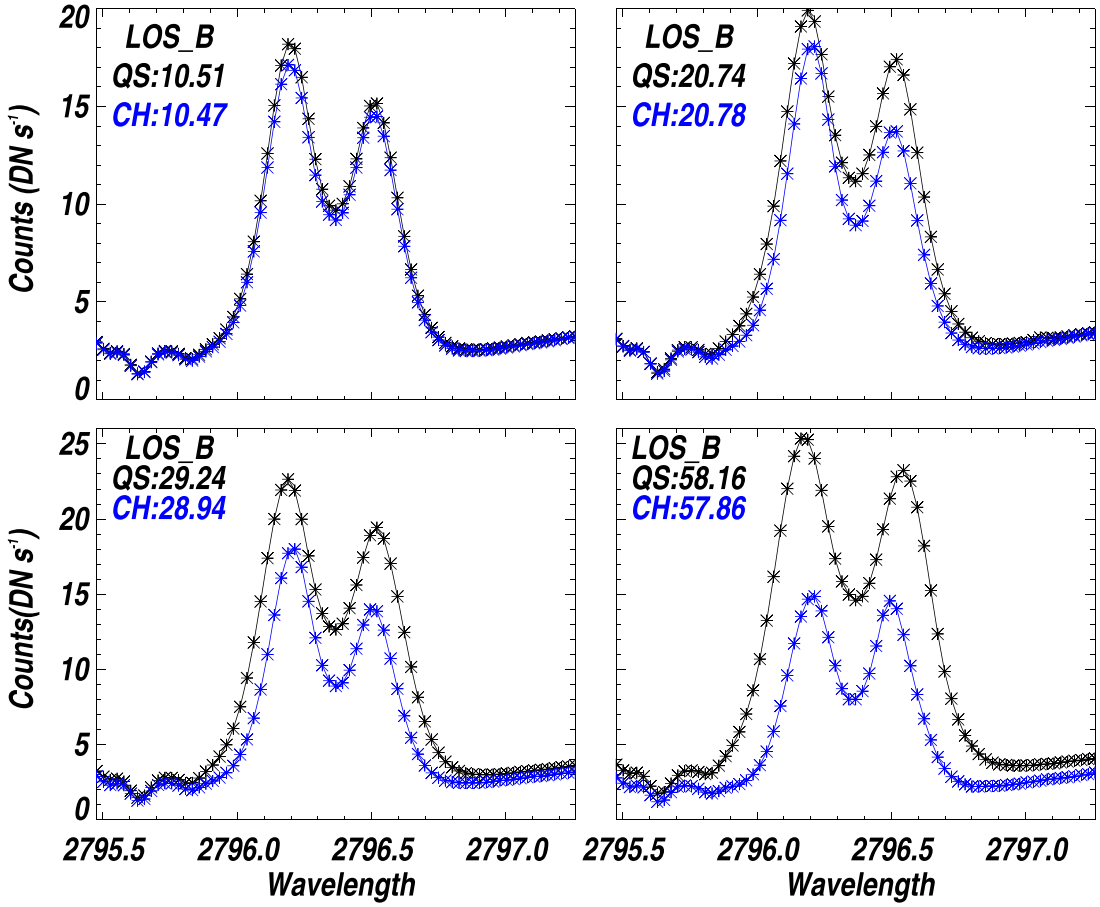

Figure 4. Mg II k line profiles averaged over the QS (black color) and CHs (blue color) in four bins of different pixel-averaged LOS magnetic field, as labeled in each panel. The values represent the average of $\langle B_{\rm LOS}\rangle/\mu$ in the respective bin. The magnetic field units are in Gauss.

heliographic coordinates ($\mu = 0.9$ both for QS and CH). The difference in the coronal intensities in QS and CH is evident from the images. Similar to case 1 studied in Section 3.1, we produce a plot of intensities in QS (black) and CH (blue) using AIA 193 Å observations as a function of $\langle B_{\rm LOS}\rangle/\mu$. It is discernible that the QS region is brighter by roughly a factor of four for areas with a similar magnetic field, similar to what was observed in case 1 (see Figure 9).

Basically, the analysis of this case confirms the results for case 1 discussed earlier. Figure 10 displays the magnetic field maps (A and D) and intensity maps obtained for k2v (B and E) and k3 (C and F) for CHs (top row) and the QS (bottom row). As can be inferred from the intensity maps, there are no apparent visual differences in CHs and QS intensities in Mg II as well as, in general, the magnetic field distribution. To perform a quantitative comparison, we produced similar plots for k3, k2v as we did for *Data Set 1*. We additionally also consider the line wing covering the wavelength range 2832.0–2834.0 Å. The spectral window for *Data Set 1* did not cover the Mg II k 2796.0 Å line wing; therefore, we could not perform the wing analysis for *set*1. Figure 11 displays the averaged intensity in each bin of $\langle B_{\rm LOS}\rangle/\mu$ for k3 (top), k2v (middle), and wing (right) of the Mg II line. These plots reveal that the average QS intensities of k3 and k2v are larger than those for CH. The difference in the intensities increases with increasing magnetic field for k3, but that is not seen for k2v.

In principle, the difference in Mg II intensity between the QS and CHs (at the same magnetic field) could also be due to an instrumental effect. One candidate could be stray light. Also there could be another hitherto unknown process that would explain the difference in physical properties of the QS and CH chromosphere of the Sun. To test that there is no hidden bias we investigate the wing of the Mg II k line (i.e., integrated emission between 2832 and 2834 Å). The wing of the Mg II k line represents the solar photosphere, where QS and CH intensities are very similar in the QS and CHs. The bottom panel of Figure 11 displays the same as the top and middle panels, but for the line wing. The overlap between CH and QS intensities is remarkable. If there are any differences between the two, then the CH actually appears slightly brighter than the QS at similar magnetic flux. Therefore, we conclude that the difference between CHs and the QS seen in the k3 and k2v components of the line is not due to some hidden bias or instrumental effect.

3.3. Effects of Spectral Resolution

Our analysis has demonstrated that there is a significant difference in narrowband Mg II k line core intensities between CH and QS. In this section, we follow two aims. First, we investigate if the difference is revealed mainly by means of the unprecedented spectral resolution that is being provided by the *IRIS* spacecraft. Second, we want to check if CHs may influence the widely used Mg II core-to-wing ratio (c/w), also known as the Mg II index (see, e.g., Heath & Schlesinger 1986). For this purpose, we consider two scenarios. In the first

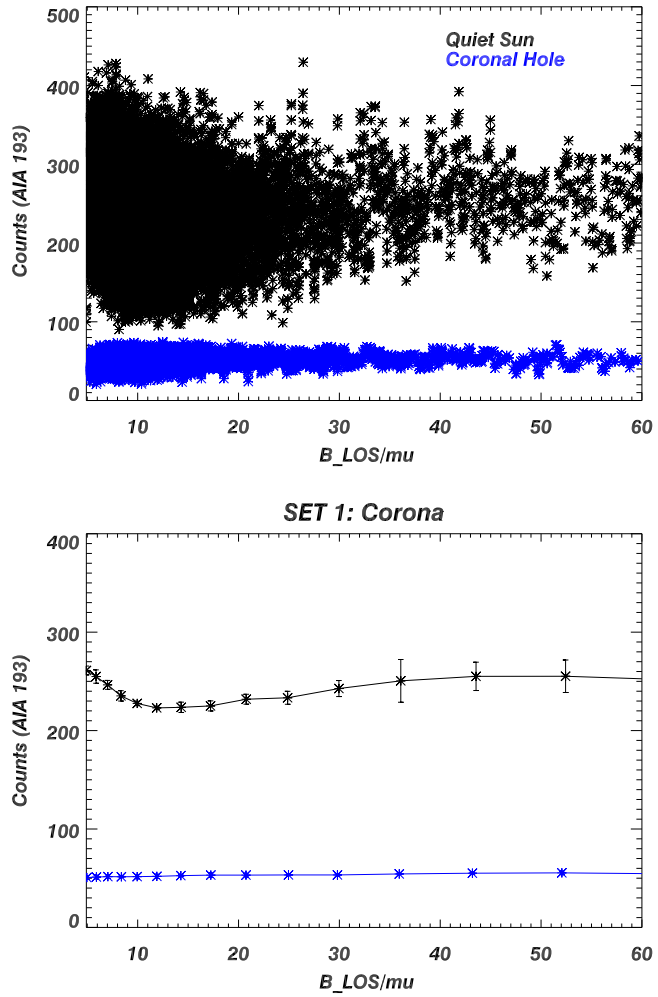

Figure 5. Coronal intensities vs. magnetic field. Top panel: intensity scatter plot as a function of magnetic field for the QS (black) and CHs (blue) as obtained using AIA 193 Å. Bottom panel: AIA 193 Å intensity averaged over bins of $\langle B_{\rm LOS}\rangle/\mu$ in the QS (black) and CHs (blue).

scenario, we degrade the *IRIS* spectra to a resolution of 1 Å, which is the spectral resolution of the SOLar-STellar Irradiance Comparison Experiment (McClintock et al. 2005) on board SOLar Radiation and Climate Experiment (Rottman 2005) data used to determine the Mg II index, and in the second scenario to 11 Å, corresponding to the spectral resolution of the Solar Backscattered UltraViolet version 2 (SBUV/2; Frederick et al. 1986; Cebula et al. 1992) on NOAA 16–18 data using a Gaussian smoothing function. After degrading the original *IRIS* spectra to 1 and 11 Å, the k2 and k3 features merge and cannot be well separated. The QS and CH intensities for each magnetic field bin are computed using the peak of each degraded spectrum for the 1 Å scenario. However, for the 11 Å spectra, the intensities are estimated by taking the average at three different wavelength locations as suggested by Heath & Schlesinger (1986). To improve the statistics, we used all three data sets listed in Table 1. For this purpose, we computed the intensities at the peak (1 Å case) and at three different points (11 Å case) and obtained an average of intensities within corresponding bins of $\langle B_{\rm LOS}\rangle/\mu$. In order to increase the statistics, we have added all three data sets described in Table 1.

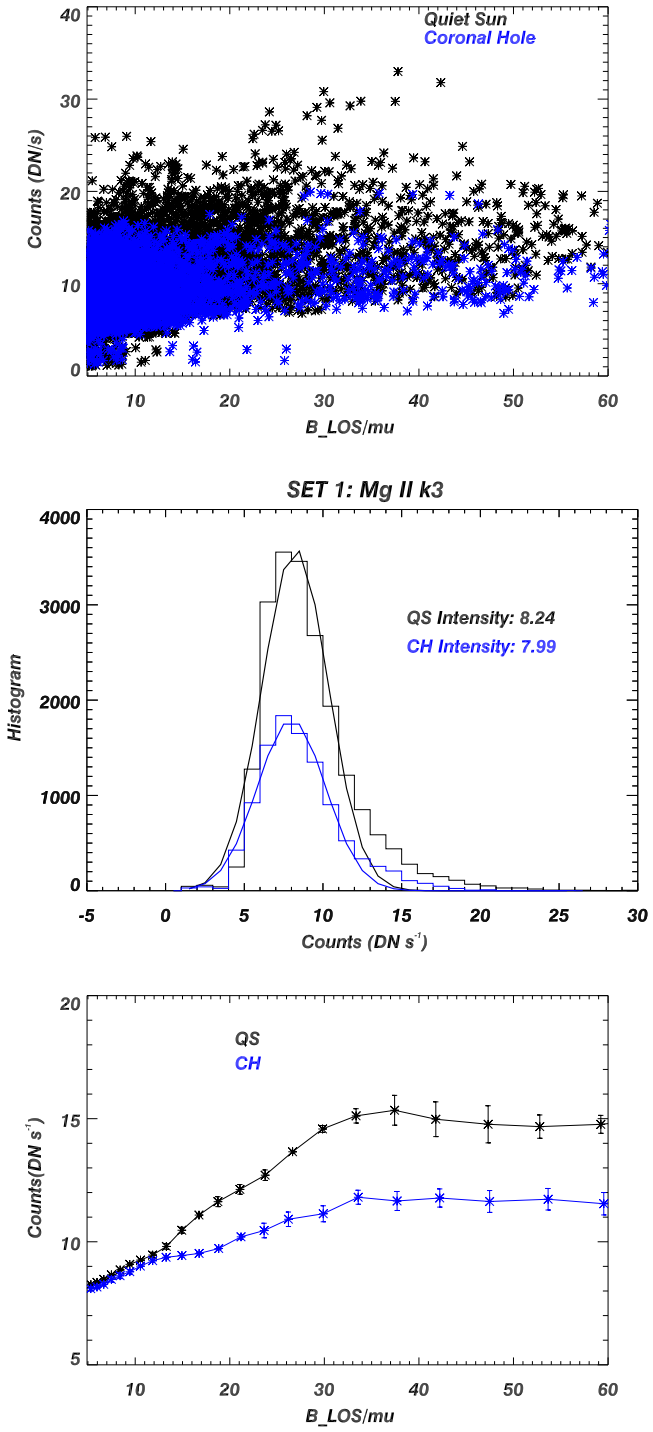

Figure 6. Chromospheric intensity in Mg II k3 vs. magnetic field. Scatter plot (top), histogram (middle), and averaged intensities with magnetic field (i.e., B/μ) of the QS (black) and CHs (blue) for Mg II k3 (bottom).

We repeat the original analysis performed on *Data Set 2*, but now with reduced spectral resolution. Figure 12 shows the QS (black) and CH (blue) intensities averaged over magnetic field bins for 1 Å (top panel) and 11 Å resolution (bottom panel). These plots reveal that for 1 Å resolution, the differences are still significant. However, for 11 Å spectra, the difference in the intensities are minimal. While there is a significant intensity contrast between QS and CH at the original spectral resolution of *IRIS*, it is almost

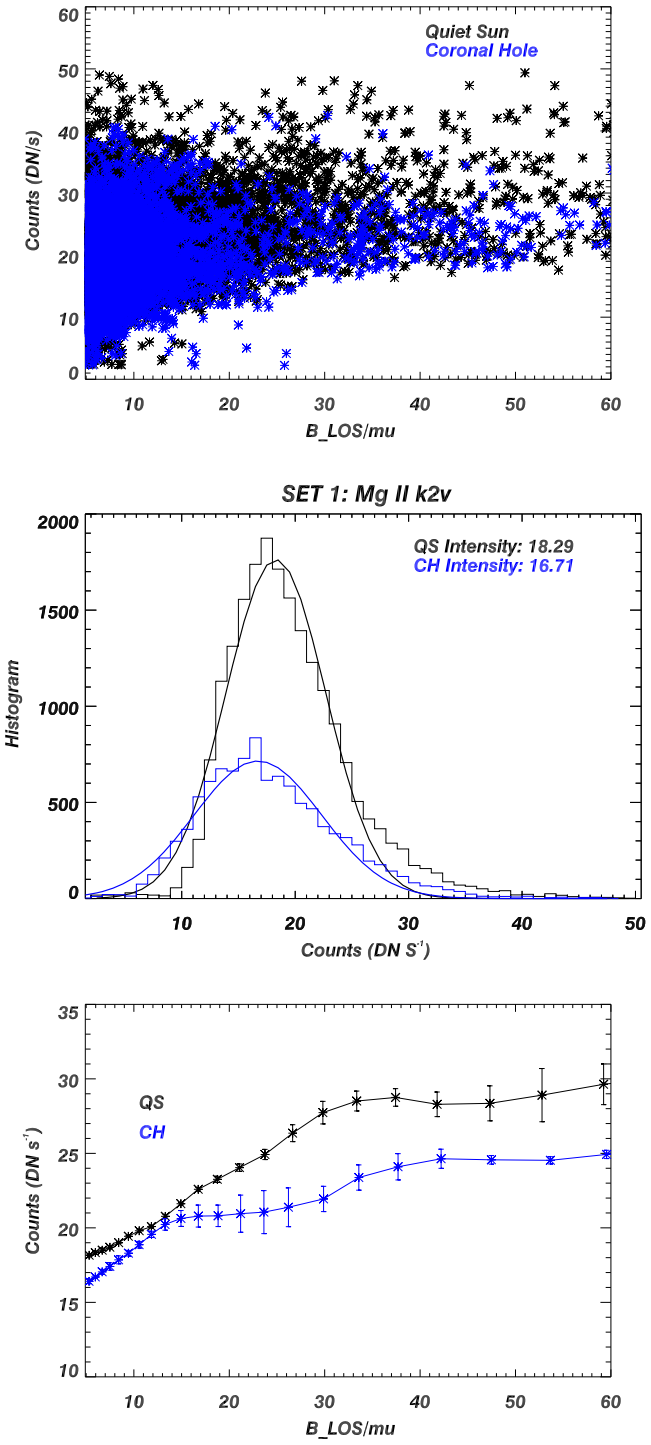

Figure 7. Same as Figure 6 but for the Mg II k2v peak intensity vs. magnetic field.

impossible to distinguish the QS and CHs at 11 Å resolution. It is noted that changes in intensity with magnetic flux density in 11 Å resolution spectra are small compared to those in 1 Å resolution spectra. This is essentially due to the fact that while calculating the intensities for 1 Å spectra the peak emission is taken, whereas, for 11 Å, the spectra averages of three different locations were taken as per the definition by Heath & Schlesinger (1986).

These results suggest that there is an influence of CHs on the Mg II c/w ratio, at least if the more recently introduced version of the Mg II index for spectral resolution of 1 Å is considered (see, e.g., Snow et al. 2005, and references therein). Since the Mg II c/w is often used as a proxy for plage areas (see, e.g., Viereck & Puga 1999), this intensity contrast between CH and QS must be taken into account in future work making use of the Mg II index, in particular, if the study is based on spectra with 1 Å resolution.

4. Discussion and Conclusions

IRIS provides high-resolution spectra of the Mg II h and k resonance lines, which are important probes of the thermal and dynamic state of the upper solar chromosphere (Leenaarts et al. 2013). The central absorption (k3) and short wavelength peak (k2v) of the Mg II k line form at different temperatures and altitudes in the solar chromosphere. In the current paper, we have studied the difference between the QS and CH intensities at different chromospheric layers using the intensities at the k2v and k3 wavelengths. Based on our analysis, we find that QS intensities in both k2v and k3 are significantly higher than those in CHs, when compared in regions of the same magnetic flux density ($\langle B_{\rm LOS}\rangle/\mu$). We also find that the difference in intensities is largest for k3, somewhat smaller for k2 and not significant in the wings of the Mg II k line. Consequently, this difference is only seen clearly if a high-resolution spectrum is used and that it decreases as the spectral resolution is lowered. Essentially, at 1 Å resolution the difference between CH and QS is still visible, but for frequently used data for deriving the Mg II index at 11 Å, it is not.

Generally, it is reported that the QS and CH start to show intensity contrast only if the temperature exceeds 6×10^5 K (Stucki et al. 2000, 2002; Wilhelm 2000; Cranmer 2009). Therefore, it is often difficult to isolate CH regions from QS without taking recourse to coronal images. The main spectral lines formed at lower temperatures that clearly show a contrast between CHs and the QS are lines of He I and He II, e.g., the He I 10830 Å absorption line (Harvey et al. 1975; Harvey & Recely 2002). However, the He I 10830 Å line is affected by coronal radiation. Also, the C IV line at 1548 Å has been reported to show a lower intensity in a polar CH (Peter 1999a).

The question arises why the intensities in QS and CH are so different in the Mg II k line core. The difference between the QS and CHs in coronal radiation was explained by Wiegelmann & Solanki (2004) by invoking loop statistics and Rosner–Tucker–Vaiana (RTV; Rosner et al. 1978) scaling. In CHs the longer loops, which reach higher altitudes and get hotter are missing. This explains why CHs are so dark compared to the QS at coronal temperatures. Shorter, less hot loops are almost as common in CHs as in the QS, which is why no (or only a small) intensity contrast between CH and QS is expected for the chromosphere. However, we note that this explanation is not directly applicable in the chromosphere due to the fact that the RTV scaling used in that paper does not apply. Further work is required to explain the difference in Mg II core brightness in CHs and the QS.

The c/w of the Mg II lines, known as the Mg II-index (see, e.g., Heath & Schlesinger 1986) are taken as a proxy for solar activity in modeling the total and spectral solar irradiance (total solar irradiance (TSI) and SSI), in particular in plage areas. In

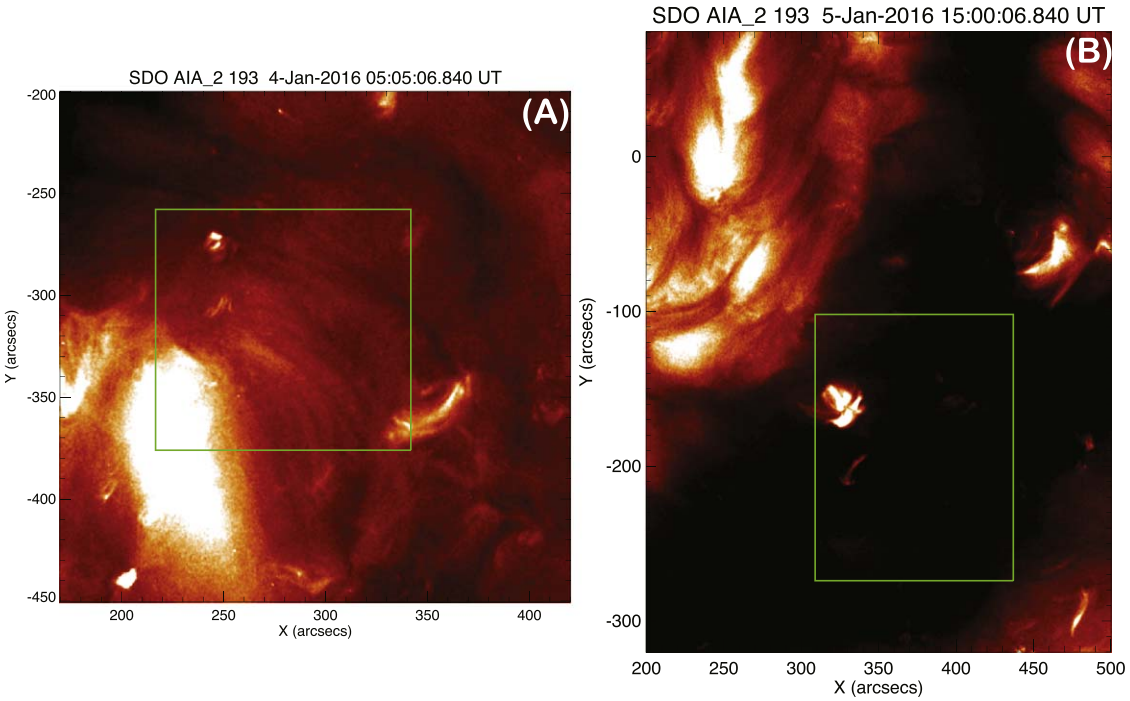

Figure 8. Region of interest for data set 2. Images taken by AIA in the 193 Å channel showing QS (left panel) and CH (right panel). The overplotted green boxes locate the regions that were rastered by *IRIS*. Note that we have used the same minimum and maximum values to plot these images.

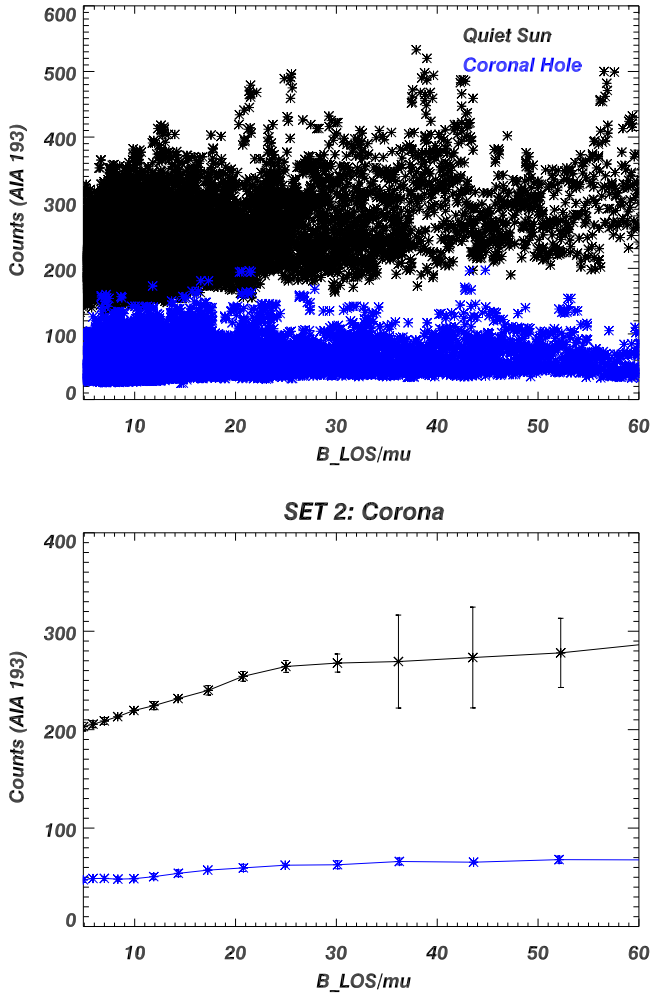

Figure 9. Same as Figure 5 but for case 2, showing coronal intensity vs. magnetic field.

the past, the index has been derived using 11 and 1 Å resolution spectra that were obtained considering Sun-as-a-star data (see, e.g., Heath & Schlesinger 1986; de Toma et al. 1997; Viereck et al. 2001; Snow et al. 2005, 2014). Our findings suggest that the Mg II index for CHs should be lower than in QS, in particular for 1 Å resolution data. This fact has not been accounted for in the modeling of the TSI or SSI using the Mg index so far. In the future, the Solar Ultraviolet Imaging Telescope (Ghosh et al. 2016; Tripathi et al. 2017) on board the Aditya-L1 mission of the Indian Space Research Organisation shall provide full disk images of the Sun in 11 different passbands in the 2000–4000 Å wavelength range, including two filters centered at the Mg II h and k lines and two at their wings. The images in the Mg II h and k lines and their wings will be obtained with a spectral resolution of 4 Å. These observations will for the first time, provide opportunities to measure the spatially resolved Mg II indices for the whole Sun, which has not been possible so far. This in turn will provide improved empirical models of the TSI as well as SSI.

We thank the anonymous referee for constructive comments. This research is supported by the Max-Planck Partner Group of MPS at IUCAA that is funded by MPG and DST (IGSTC). *IRIS* is a NASA small explorer mission developed and operated by LMSAL with mission operations executed at NASA Ames Research center and major contributions to downlink communications funded by ESA and the Norwegian Space Centre. AIA and HMI data are courtesy of NASA/*SDO* and the AIA and HMI science teams. This work was partly supported by the BK21 plus program through the National Research Foundation (NRF) funded by the Ministry of Education of Korea. P.K. is currently funded through the National Science Centre, Poland, (NCN) grant No. 2014/15/B/ST9/00106.

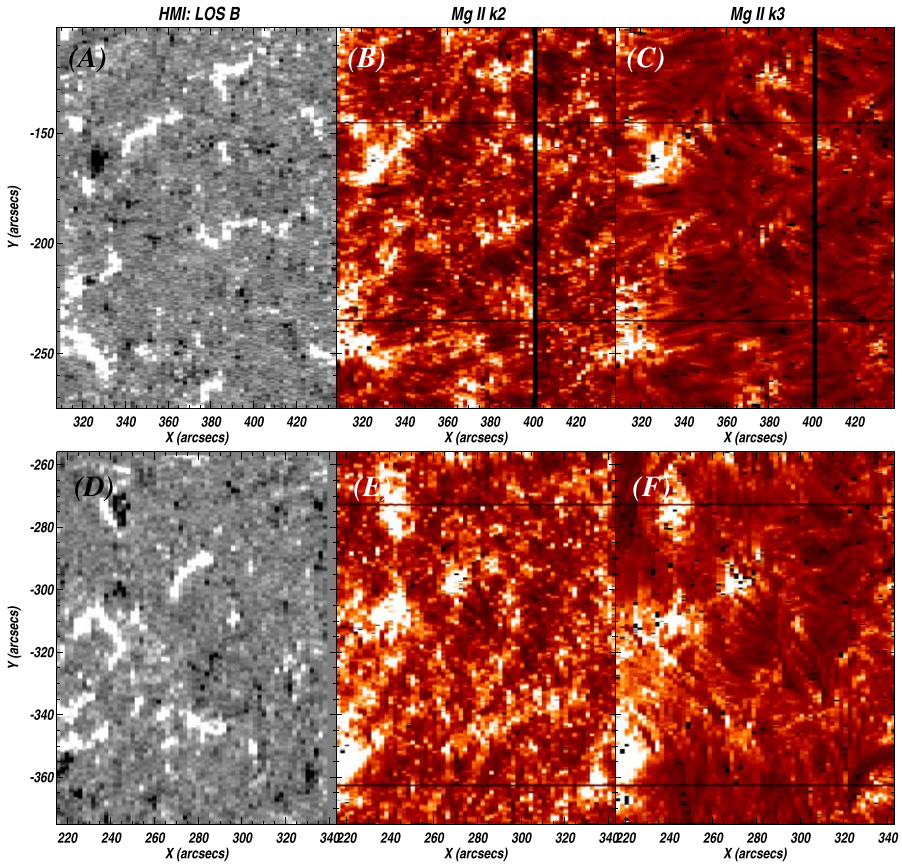

Figure 10. Photospheric magnetic field and chromospheric emission for data set 2. Magnetograms are shown in panels (A) and (D), Mg II k2v maps are shown in panels (B) and (E) and k3 maps are shown in panels (C) and (F). Top row is for CHs and bottom row is for the QS.

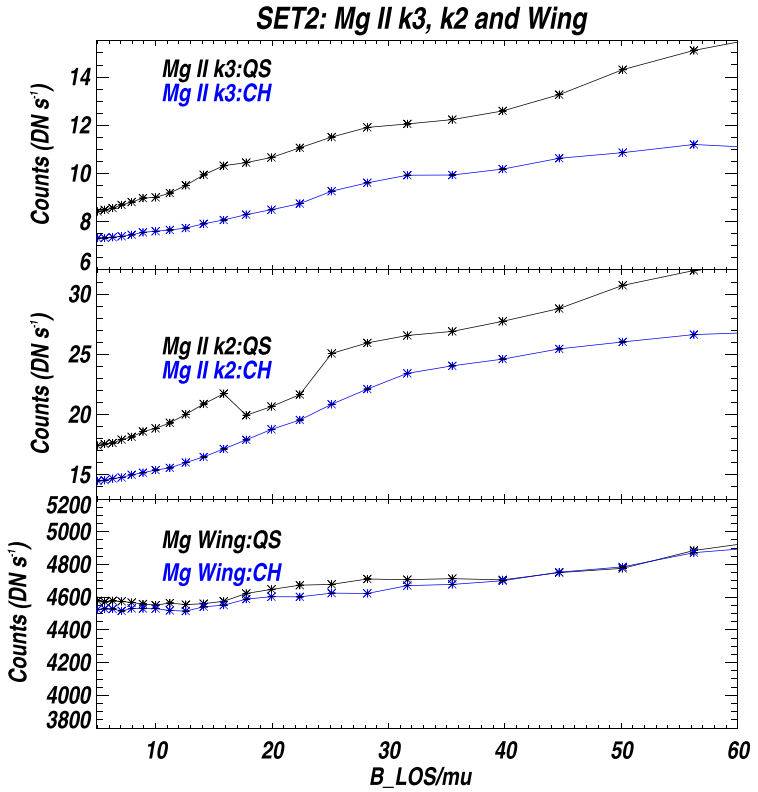

Figure 11. Relation of chromospheric emission to magnetic field for data set 2. Average intensities obtained in Mg II k3 (top panel), k2 (middle panel), and wing as a function of $\langle B_{\rm LOS}\rangle/\mu$.

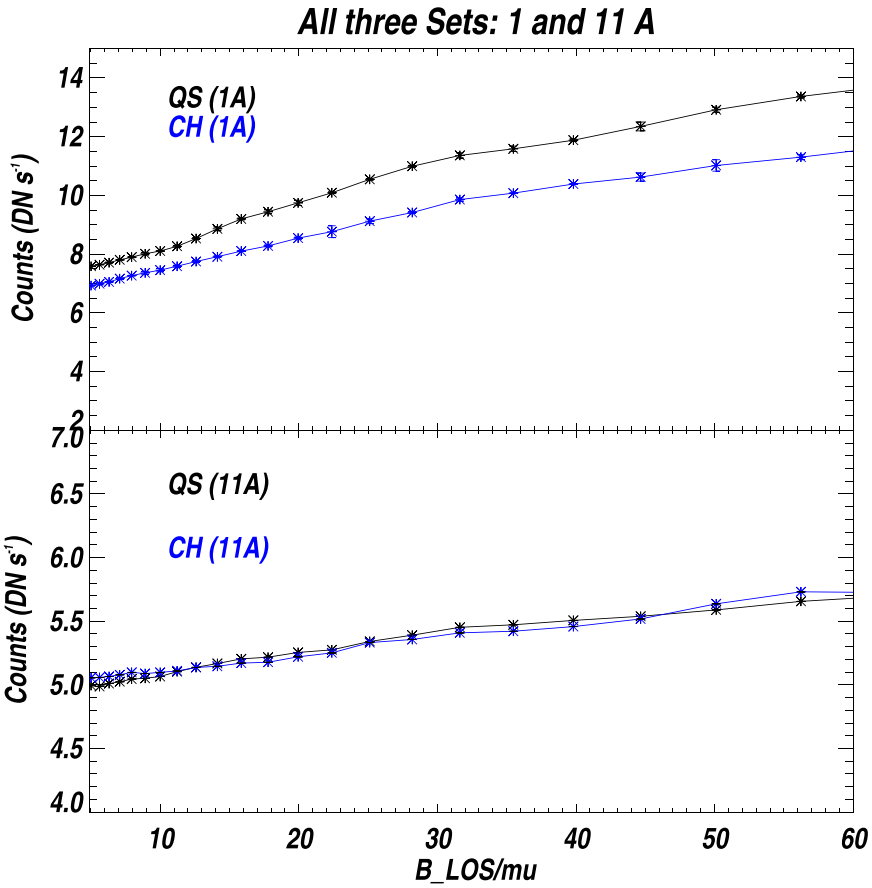

Figure 12. Intensity vs. magnetic field based on low spectral resolution data. QS (black) and CH (blue) intensities as a function of magnetic field estimated using 1 Å spectra (top panel) and 11 Å spectra (bottom panel).

Appendix
Data Set 3: The Observations on 2014 November 29 and December 18

Here we present the results obtained from date set 3 as listed Table 1. The QS observation is an 18 step coarse raster with an exposure time of 30 s, while the CH observation is a 64 step coarse raster with an exposure time of 15 s. The μ range covered in the CH study is rather large (0.449–0.659) as compared to that of the QS (0.471–0.539). Therefore, the analysis was performed to only a selected part of the QS study where the μ values overlapped. The FOV for this case are shown in Figure 13 and the resulting chromospheric emission versus magnetic field is displayed in Figure 14.

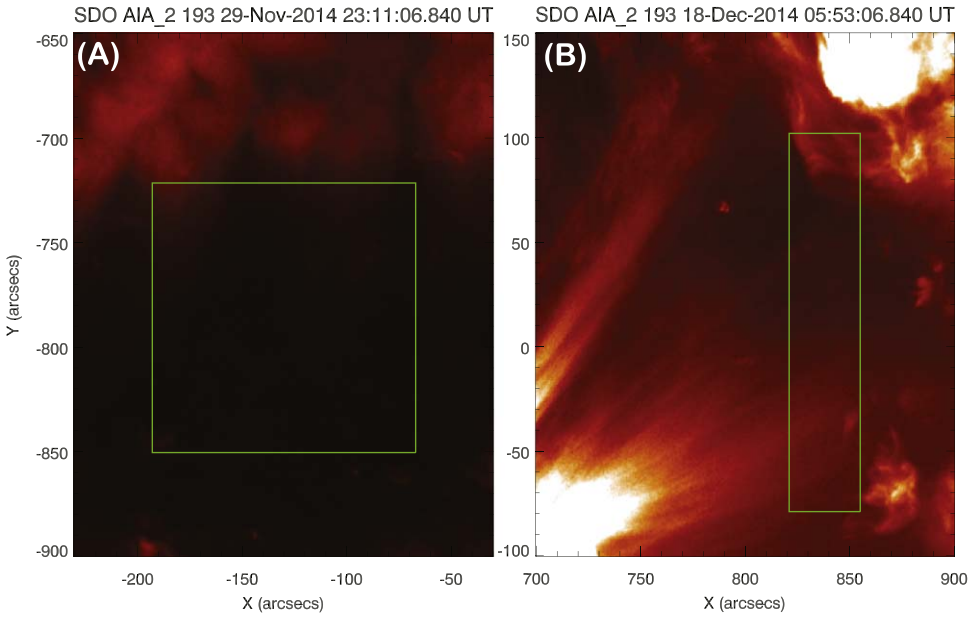

Figure 13. Fields of view for data set 3 as seen in the 193 Å channel of AIA (similar to Figure 8).

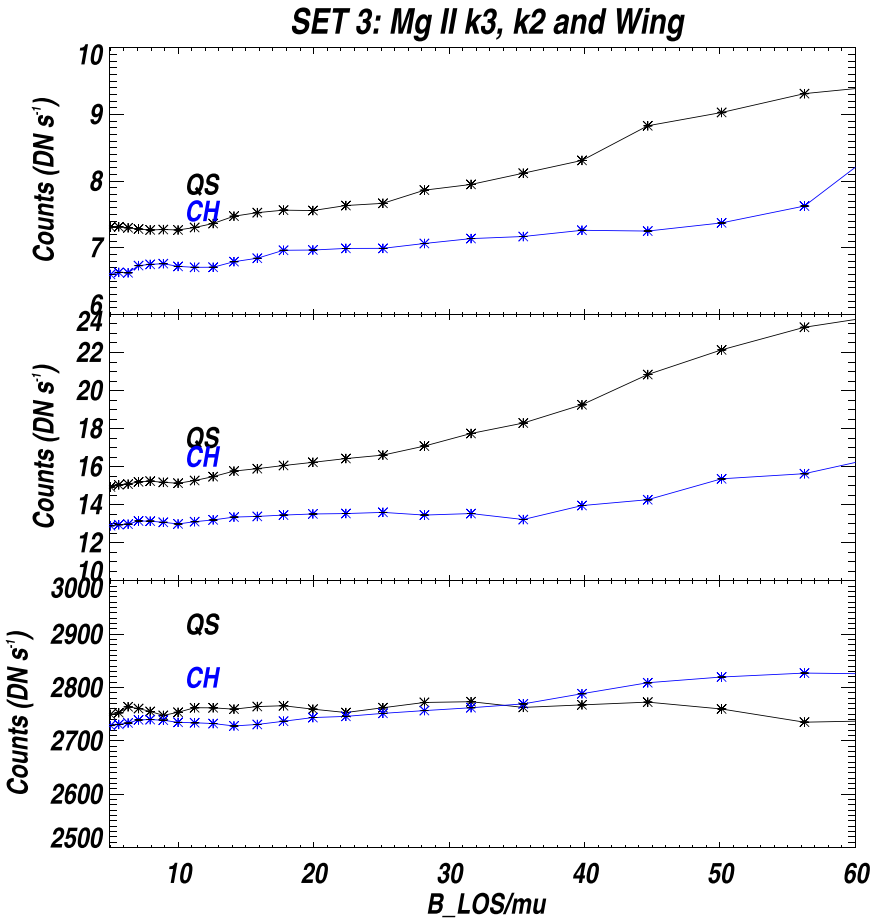

Figure 14. Same as Figure 11 but for data set 3.

ORCID iDs

Durgesh Tripathi https://orcid.org/0000-0003-1689-6254

References

Andretta, V., & Jones, H. P. 1997, ApJ, 489, 375
Avrett, E. H., Fontenla, J. M., & Loeser, R. 1994, in IAU Symp. 154, Infrared Solar Physics, ed. D. M. Rabin, J. T. Jefferies, & C. Lindsey (Dordrecht: Kluwer), 35
Avrett, E., Landi, E., & McKillop, S. 2013, ApJ, 779, 155
Cebula, R. P., Deland, M. T., & Schlesinger, B. M. 1992, JGR, 97, 11613
Centeno, R., Trujillo Bueno, J., Uitenbroek, H., & Collados, M. 2008, ApJ, 677, 742
Cranmer, S. R. 2009, LRSP, 6, 3
De Pontieu, B., Title, A. M., Lemen, J. R., et al. 2014, SoPh, 289, 2733
de Toma, G., White, O. R., Knapp, B. G., Rottman, G. J., & Woods, T. N. 1997, JGR, 102, 2597
Dupree, A. K., Penn, M. J., & Jones, H. P. 1996, ApJL, 467, L121
Frederick, J. E., Heath, D. F., & Cebula, R. P. 1986, JAtOT, 3, 472
Ghosh, A., Chatterjee, S., Khan, A. R., et al. 2016, Proc. SPIE, 9905, 990503
Gouttebroze, P., & Lemaire, P. 1974, A&A, 34, 375
Harrison, R. A., Sawyer, E. C., Carter, M. K., et al. 1995, SoPh, 162, 233
Harvey, J. W., Krieger, A. S., Davis, J. M., Timothy, A. F., & Vaiana, G. S. 1975, BAAS, 7, 358
Harvey, K. L., & Recely, F. 2002, SoPh, 211, 31
Heath, D. F., & Schlesinger, B. M. 1986, JGR, 91, 8672
Leenaarts, J., Golding, T., Carlsson, M., Libbrecht, T., & Joshi, J. 2016, A&A, 594, A104
Leenaarts, J., Pereira, T. M. D., Carlsson, M., Uitenbroek, H., & De Pontieu, B. 2013, ApJ, 772, 90
Lemen, J. R., Title, A. M., Akin, D. J., et al. 2012, SoPh, 275, 17
McClintock, W. E., Rottman, G. J., & Woods, T. N. 2005, SoPh, 230, 225
Pereira, T. M. D., Leenaarts, J., De Pontieu, B., Carlsson, M., & Uitenbroek, H. 2013, ApJ, 778, 143
Peter, H. 1999a, ApJ, 516, 490
Peter, H. 1999b, ApJL, 522, L77
Rosner, R., Tucker, W. H., & Vaiana, G. S. 1978, ApJ, 220, 643
Rottman, G. 2005, SoPh, 230, 7
Scherrer, P. H., Schou, J., Bush, R. I., et al. 2012, SoPh, 275, 207
Schmit, D., Bryans, P., De Pontieu, B., et al. 2015, ApJ, 811, 127
Snow, M., McClintock, W. E., Woods, T. N., et al. 2005, SoPh, 230, 325
Snow, M., Weber, M., Machol, J., Viereck, R., & Richard, E. 2014, JSWSC, 4, A04
Stucki, K., Solanki, S. K., Pike, C. D., et al. 2002, A&A, 381, 653
Stucki, K., Solanki, S. K., Schühle, U., et al. 2000, A&A, 363, 1145
Teplitskaya, R. B., Ozhogina, O. A., & Turova, I. P. 2006, AstL, 32, 120
Teplitskaya, R. B., Turova, I. P., & Ozhogina, O. A. 2007, SoPh, 243, 143
Tripathi, D., Ramaprakash, A. N., Khan, A. R., et al. 2017, CSci, 113, 616
Viereck, R., Puga, L., McMullin, D., et al. 2001, GeoRL, 28, 1343
Viereck, R. A., & Puga, L. C. 1999, JGR, 104, 9995
Waldmeier, M. 1975, SoPh, 40, 351
Wiegelmann, T., & Solanki, S. K. 2004, SoPh, 225, 227
Wilhelm, K. 2000, A&A, 360, 351
Wilhelm, K., Dammasch, I. E., Marsch, E., & Hassler, D. M. 2000, A&A, 353, 749
Wilhelm, K., Curdt, W., Marsch, E., et al. 1995, SoPh, 162, 189